

Supporting Information

Spider Toxin Peptide Lycosin-I Functionalized Gold Nanoparticles for *in vivo* Tumor Targeting and Therapy

Huaxin Tan,^{†,‡,¶} Yazhou Huang,[†] Jianghong Xu,[‡] Bo Chen,[‡] Peng Zhang,[†] Zhongju Ye,[‡] Songping Liang,[†] Lehui Xiao,^{*,‡,§} and Zhonghua Liu^{*,†}

[†] The National & Local Joint Engineering Laboratory of Animal Peptide Drug Development, College of Life Sciences, Hunan Normal University, Changsha, Hunan 410081, China

[‡] Key Laboratory of Phytochemical R&D of Hunan Province, College of Chemistry and Chemical Engineering, Hunan Normal University, Changsha, Hunan, 410081, P. R. China

[§] State Key Laboratory of Medicinal Chemical Biology College of Chemistry, Tianjin Key Laboratory of Biosensing and Molecular Recognition, Nankai University, Tianjin, 300071, China

[¶] Department of Biochemistry and Molecular Biology, School of Pharmaceutical and Biological Science, University of South China, Hengyang, 421001, China

*Corresponding authors

E-mail: Lehui Xiao, lehuixiao@nankai.edu.cn; Zhonghua Liu, liuzh@hunnu.edu.cn

Experimental Section

Materials and Cell Lines.

HAuCl₄·3H₂O, cetyltrimethylammonium bromide (CTAB), NaBH₄, and NaCl were purchased from Sinopharm Chemical (Shanghai, China). Dynasore, genistein, Bis-(p-sulfonatophenyl)phenylphosphine dehydrate dipotassium (BSPP), 4, 7, 10, 13, 16, 19, 22, 25, 32, 35, 38, 41, 44, 47, 50, 53-Hexadeca-28, 29-dithiahexapentacontanedioic acid di-N-succinimidyl ester (SH-PEG-NHS, C₄₆H₈₀N₂O₂₄S₂, MW:1109) and O-[2-(3-Mercaptopropionylamino)ethyl]-O'-methylpolyethylene glycol (SH-PEG-CH₃, CH₃O(CH₂CH₂O)_nCH₂CH₂SH, MW: 5000) were obtained from Sigma-Aldrich (St. Louis, MO, U.S.A.). Tat peptide (sequence, YGRKKRRQRRR) was purchased from AnaSpec. (San Jose, CA, U.S.A.). Lycosin-I were synthesized by solid phase synthesis method as we described previously [1]. All other chemicals not mentioned here were purchased from Sigma-Aldrich. Human cervical carcinoma HeLa cells, mouse prostatic carcinoma Mat-LyLu cells, human colon carcinoma SW480 cells, human mammary epithelial HBL-100 cells, human vascular endothelial Huvec cells and human embryonic kidney Hek293t cells were cultured in DMEM medium (GIBCO) supplemented with 10% fetal bovine serum (GIBCO), 1% penicillin and streptomycin at 37 °C in humidified air containing 5% CO₂. The primary cardiocytes and hippocampus neuron were acutely isolated from neonatal mice as we described previously [2, 3].

Synthesis and characterization of LGNPs and LGNRs

The modification strategies to synthesize LGNPs and LGNRs were shown in **Fig.S1A**. GNP solutions showed a slight red shift of 2 nm (p value=0.018) in absorption maxima after binding to lycosin-I, indicating the success of peptide modification to GNPs (**Fig.S1B, upper**). This is further confirmed by the increase of Zeta-potential from -53.32±2.54 mV to -33.28±4.37 mV (**Fig.S1C, upper**). Additionally, no aggregates were formed during the modification process as reflected in the UV-vis absorption spectra of GNP solutions before and after lycosin-I coating, which was also confirmed by the negligible size change of GNPs after peptide modification as shown in **Fig.S1C**.

We also established the lycosin-I-modified gold nanorods (LGNRs) system by using similar modification strategy. The fabricated GNRs were characterized by DLS with approximated size of 65.80±3.18 nm (measured by TEM as shown in **Fig.S2**), and the sizes of GNRs were barely changed by the peptide modification (**Fig.1C**). Unlike GNPs, the zeta-potentials of GNRs were 34.17±2.28 mV owing to the cationic covered CTAB ligands which were used to

stabilize the nanorods during the synthetic process. The peptide coupling increased the zeta-potentials of GNRs to 44.03 ± 1.23 mV, confirming successful conjugation of lycosin-I.

The stability of LGNPs was investigated by dark-field microscopy under different solution condition. As shown in **Fig.S3**, LGNPs presented homogeneous intensity and color, indicative of no aggregation. Likewise, the statistical distribution of scattering intensities from individual spots in different surroundings shared the similar curve features. Above all confirmed the stable monodispersity of lycosin-I conjugated nanoparticles, which is conducive to following studies in living system.

Intracellular accumulation of LGNPs in HeLa cells.

To investigate the localization of LGNPs in cells, HeLa cells containing a certain amount of LGNPs were observed by dark-field microscope at different time points. To avoid the influence of excessive LGNPs, HeLa cells were gently washed and cultured with fresh culture media after co-incubation with $16 \mu\text{g}/\text{mL}$ of LGNPs for 1 hour. The spatial distribution of internalized LGNPs in HeLa cells at various time points are shown in **Fig.S4**. Around one hour later, individual LGNP appeared inside the cytosol. With time prolonging, the number of intracellular nanoparticles gradually increased. After 3 hours, the scattering intensities of entered LGNPs became inhomogeneous, indicating the formation of LGNPs aggregates. 16 hours later, the LGNPs aggregates were concentrated and distributed mirror symmetrically in the corners of two daughter cells. The internalized LGNPs showed no distinct effect on normal cellular activities including cell division.

Cellular uptake of LGNPs in primary mammalian cells.

The uptake of functionalized GNPs was further investigated in two primary mammalian cells, rat cardiocytes and hippocampus neurons. As shown in **Fig.S5**, LGNPs stayed impermeable in those two isolated normal cells just like the PGNPs. Though TGNPs were unable to enter cardiocytes, they still possessed the high uptake efficiency in hippocampus neurons. These data further confirmed the selectivity of LGNPs intracellular translocation in cancerous cells.

Secondary structure of S-lycosin-I.

The secondary structure of S-lycosin-I was detected by circular dichroism spectrum as we described in early studies [1, 4]. Briefly, S-lycosin-I were dissolved and diluted to a final concentration of $50 \mu\text{M}$ by water and POPC-lipid ($0.5 \text{ mg}/\text{mL}$) separately. The CD spectrum of different peptide dilutions from 190 nm to 260 nm were measured at scanning speed of $200 \text{ nm}/\text{s}$ three times. Mean residue ellipticity were derived from CD millidegrees after background subtraction and smoothing. As shown in **Fig.S6**, S-lycosin-I showed a random coil structure with or without lipids, while lycosin-I displayed obvious α -helical structure in the

presence of POPC [4]. The data verified the alteration of S-lycosin-I in secondary structure compared with natural lycosin-I.

Intracellular uptake kinetics of LGNPs entering HeLa cells.

As revealed by the kinetical data of LGNPs intracellular translocation (**Fig.S7**), the intracellular uptake of LGNPs in HeLa cells was a nanoparticle concentration- and incubation time-dependent process. The intake of LGNPs will reach saturation at nanoparticle concentration of 64 $\mu\text{g}/\text{mL}$ (for 2-hour co-incubation) and at time point of 10 hours at fixed concentration.

Cell viabilities of GNPs-treated HeLa cells.

The cytotoxicity of different GNPs was tested by MTT assay. The results in **Fig.S8** confirmed the safety of LGNPs to cell viability even at the treated concentration of 128 $\mu\text{g}/\text{mL}$. These data suggested that LGNPs can effectively accumulated and aggregated in cells with no effect on cell viability, which reveals the great potential of LGNPs in drug delivery for its biocompatibility and stability in cells.

The photothermal effect of LGNRs.

As shown in **Fig.S10**, the photothermal efficiency was not affected by the conjugation of lycosin-I. After 2-minute exposure to NIR irradiation (808 nm, 5 W/cm^2), the temperature of LGNRs solution rose to around 53 $^{\circ}\text{C}$ just like bare GNRs, while blank solution without GNRs kept at room temperature of 20 $^{\circ}\text{C}$ under the same condition.

The transmission electron microscope images of LGNRs-loaded tumor cells from tumor-bearing mice.

The tumor tissues of each group in GNR-treated mice were fixed and sliced for transmission electron microscopy (TEM) examination. **Fig.S11** clearly showed the intracellular LGNRs scattered in the cytoplasm, while PGNRs were mostly clustered in vesicles with evidently reduced amounts.

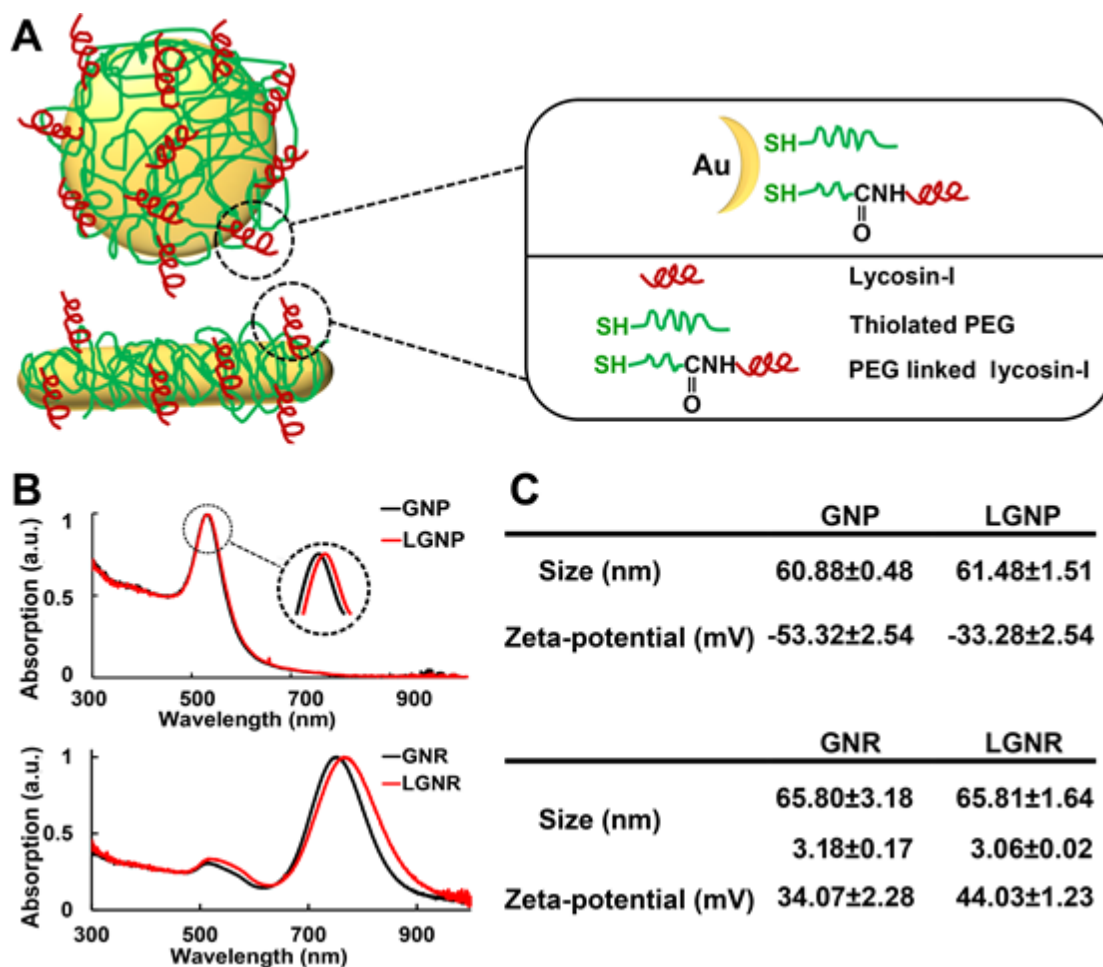


Fig.S1 A) Schematic diagram of LGNP and LGNR functionalization. B) UV-vis absorption spectra of two kinds of gold nanoparticles before (*black*) and after (*red*) lycosin-I modification. C) Sizes and zeta-potentials of two kinds of gold nanoparticles before and after lycosin-I modification (mean±SD, n=3).

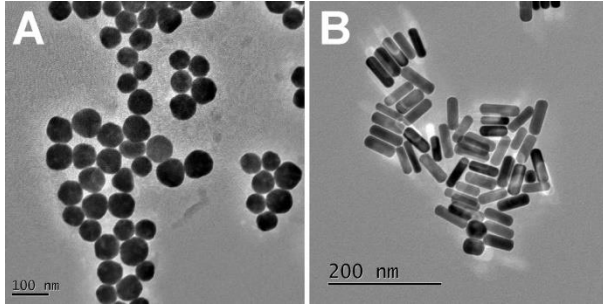


Fig.S2 TEM image of A) LGNPs and B) LGNRs.

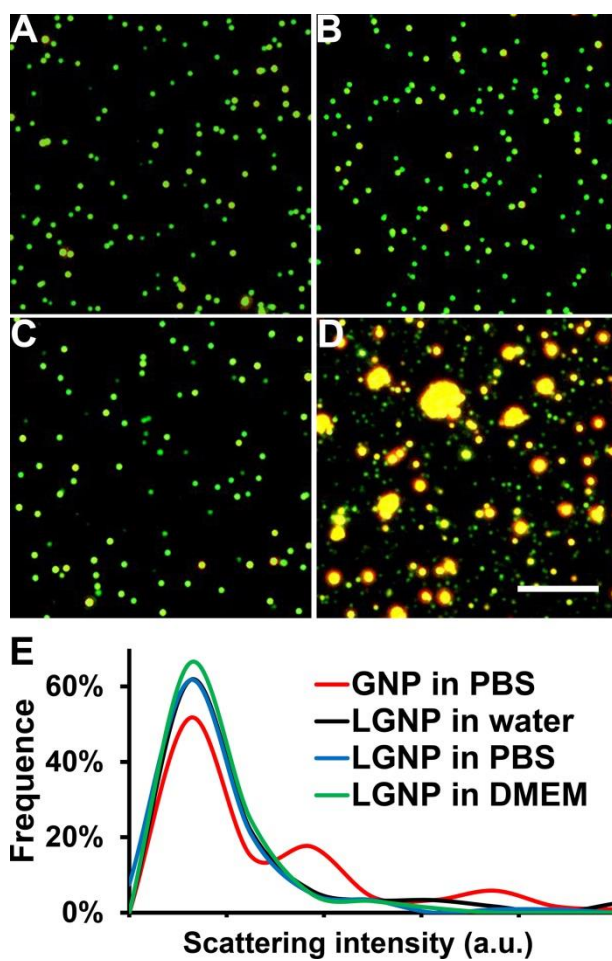


Fig.S3 Dark-field microscopic images of LGNPs in A) water, B) PBS, C) cell culture medium. D) Bare GNPs in PBS. E) Scattering intensity distributions of LGNPs in various solutions. The scale bar represents 10 μ m.

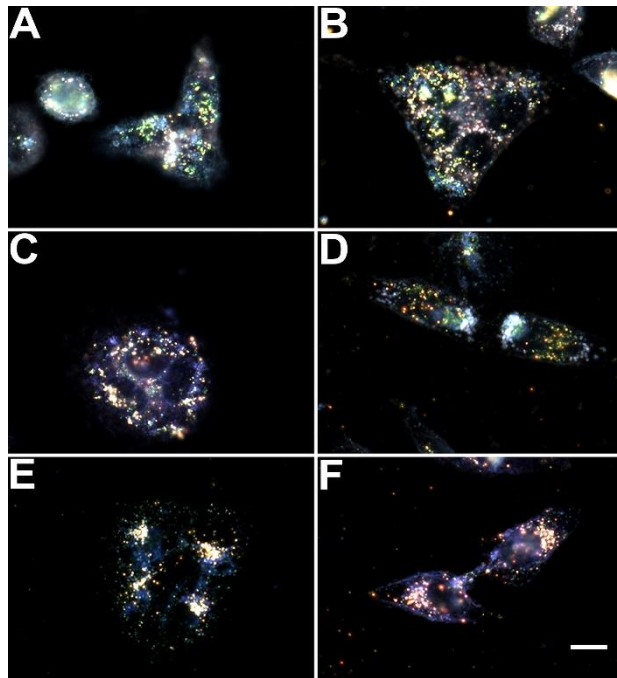


Fig.S4 Intracellular distributions of LGNPs in HeLa cells after been internalized for 1 hour (A), 3 hours (B), 6 hours (C), 12 hours (D), 16 hours (E) and 24 hours (F). The scale bar represents 10 μ m.

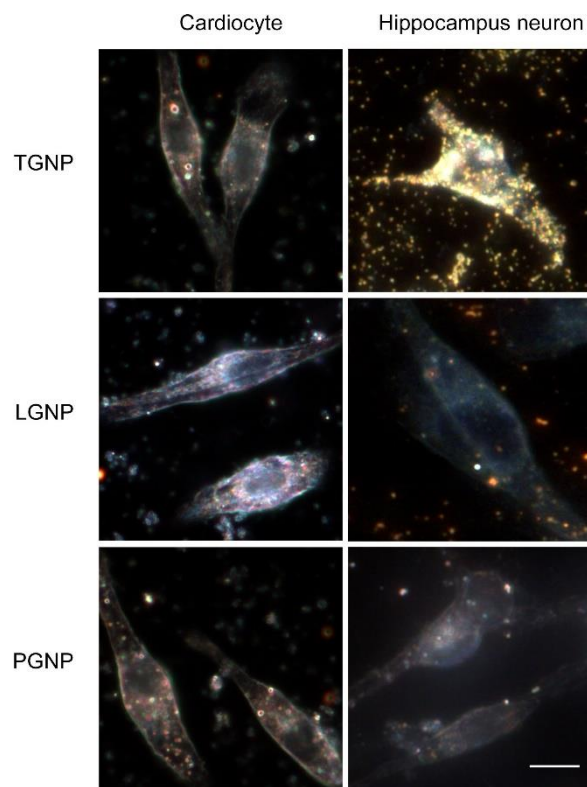


Fig.S5 Cellular uptake of LGNPs in primary mammalian cells. The scale bar represents 10 μ m.

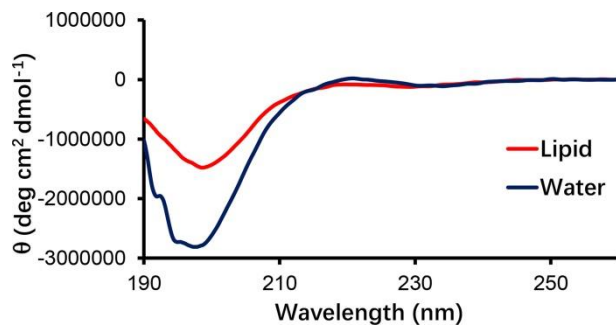


Fig.S6 Secondary structure of S-lycosin-I. Circular dichroism spectrometry of S-lycosin-I in water with or without or POPC lipids.

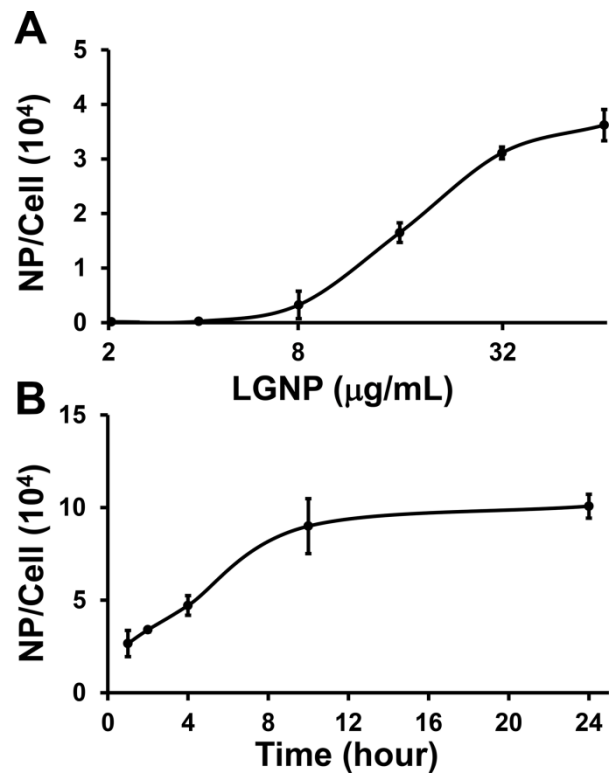


Fig.S7 A) Quantitative analysis of cellular intake of LGNPs in HeLa cells under different LGNPs concentration. B) Time growth curve of cellular internalized LGNPs in HeLa cells. (mean \pm SD, n=3)

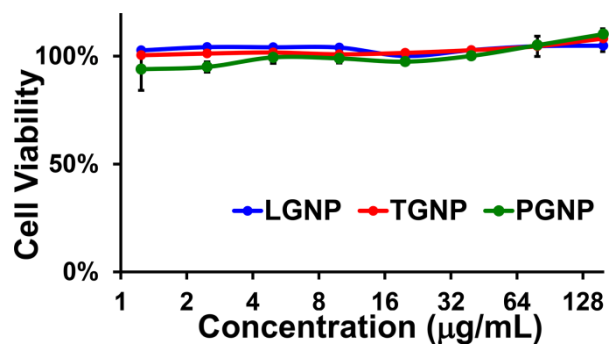


Fig.S8 Cell viability assay of three kinds of GNPs against HeLa cells (mean±SD, n=3).

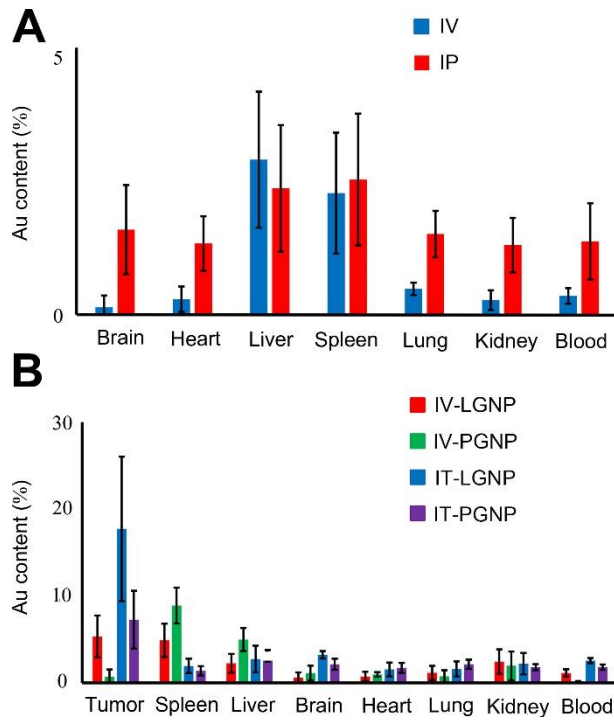


Fig.S9 The ratios of LGNPs accumulation *in vivo*. A) Bio-distribution of LGNPs in normal mice. B) Bio-distribution of LGNPs in tumor-bearing mice. Nanoparticles were injected into mice via administration routes of intravenous (IV), intratumor (IT) or intraperitoneal (IP) injection (mean \pm SD, n=5) with 200 μ g per mouse.

μg	IV	IP
Brain	0.27±0.44	3.18±1.67
Heart	0.58±0.47	2.66±1.01
Liver	5.81±2.55	4.73±2.37
Spleen	4.56±2.26	5.07±2.47
Lung	0.97±0.23	3.03±0.86
Kidney	0.55±0.36	2.62±1.02
Blood	0.71±0.29	2.76±1.43

Table.S1 The absolute contents of LGNPs in normal mice.

μg	IV-LGNP	IT-LGNP	IT-PGNP	IV-PGNP
Tumor	10.66±4.82	35.43±16.63	14.52±6.66	1.37±1.70
Spleen	9.78±3.85	3.90±1.66	2.76±1.08	17.77±4.13
Liver	4.49±2.14	5.49±3.06	6.22±1.29	9.95±2.66
Brain	1.20±1.20	6.46±0.82	4.27±1.26	2.26±1.68
Heart	1.45±1.10	3.07±1.61	3.44±1.17	1.93±0.53
Lung	2.29±1.63	3.18±1.73	4.28±1.04	1.51±1.38
Kidney	4.86±2.83	4.42±2.45	3.60±0.67	3.91±3.30
Blood	2.26±0.82	5.11±0.58	3.60±0.60	0.28±0.14

Table.S2 The absolute contents of LGNPs and PGNPs in tumor-bearing mice.

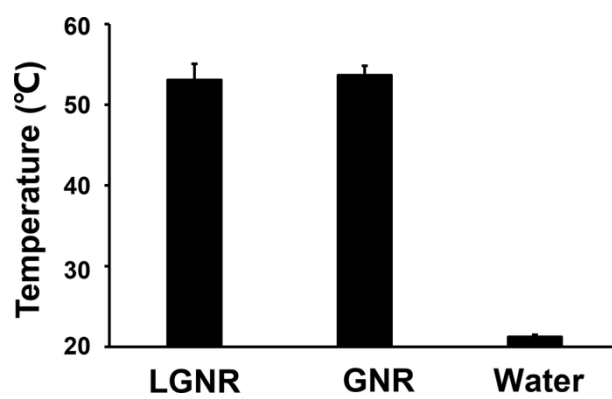


Fig.S10 Temperature increase of water solutions with and without GNRs after NIR irradiation (808 nm, 5W/cm²).

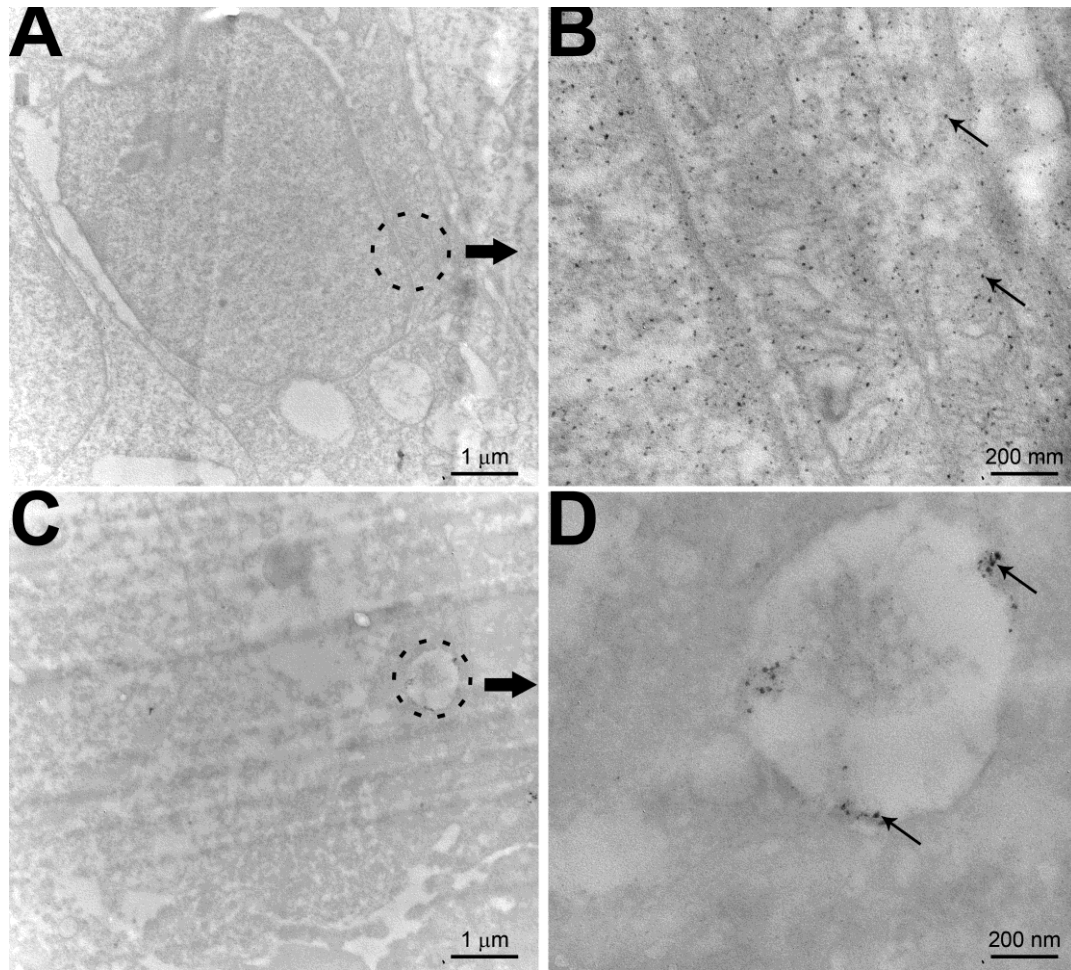


Fig.S11 Transmission electron microscopy images of tumor tissues from LGNRs (A and B) and PGNRs (C and D) treated mice. The tilted arrows indicate gold nanoparticles. (Mic JEM-1200, HV: 80 kV, magnification: 20000× for A-B, 100000× for B-C)

References

1. Liu Z, Deng M, Xiang J, Ma H, Hu W, Zhao Y, et al. A novel spider peptide toxin suppresses tumor growth through dual signaling pathways. *Curr Mol Med*. 2012; 12: 1350-1360.
2. Xiao Y, Tang J, Yang Y, Wang M, Hu W, Xie J, et al. Jingzhaotoxin-III, a novel spider toxin inhibiting activation of voltage-gated sodium channel in rat cardiac myocytes. *J Biol Chem*. 2004; 279: 26220-26226.
3. Wang RL, Yi S, Liang SP. Mechanism of action of two insect toxins huwentoxin-III and hainantoxin-VI on voltage-gated sodium channels. *J Zhejiang Univ Sci B*. 2010; 11: 451.
4. Tan H, Luo W, Wei L, Chen B, Li W, Xiao L, et al. Quantifying the Distribution of the Stoichiometric Composition of Anticancer Peptide Lycosin-I on the Lipid Membrane with Single Molecule Spectroscopy. *J Phys Chem B*. 2016; 120: 3081-3088.